IEEE Access
Multidisciplinary | Rapid Review | Open Access Journal

Received 22 November 2023, accepted 28 December 2023, date of publication 8 January 2024, date of current version 24 January 2024.

Digital Object Identifier 10.1109/ACCESS.2024.3351565

RESEARCH ARTICLE

A Simple Approach to Detect High Impedance Fault Using Morphological Gradient Edge Detector

MOSLEM SALEHI[1], MAHDI ZOLFAGHARI[2], (Member, IEEE), AND JACQUES M. MARITZ[3]

[1]Department of Electrical Engineering, Technical and Vocational University (TVU), Tehran 1435761137, Iran
[2]Department of Electrical Engineering, Amirkabir University of Technology, Tehran 1591634311, Iran
[3]Department of Engineering Sciences, University of the Free State, Bloemfontein 9301, South Africa

Corresponding author: Jacques M. Maritz (maritzjm@ufs.ac.za)

ABSTRACT Detection of high impedance faults (HIF) is one of the biggest challenges in power distribution networks. HIF usually occurs when conductors in the distribution network are broken and accidently come into contact the ground or a tree branch. The current of this fault is close to the load current level and cannot be detected by overcurrent relays. Also, some regular system phenomena such as capacitor switching, load switching, and inrush current and saturation phenomena in current transformer (CT) represent some features which may overlap the components of HIF; making HIF detection schemes more complex. In this paper, a new method for HIF detection is presented which is able to distinguish any type of HIF from regular system phenomena. To achieve this, the scheme of morphological gradient edge detection (MGED) is used to process voltage signals. The MGED extracts two main features from the processed signals: first, the edges or changes in the signal are elicited and then, these features are extracted after two cycles from the onset of the fault. Then, based on these features, a high impedance fault detection index (HIFDI) is introduced for distinguishing and classifying HIF from other regular system phenomena. The simulation results for different types of HIF fault in a sample 20 kV distribution feeder and IEEE 34-bus distribution test system using EMTP confirm the fast and accurate performance of the proposed method.

INDEX TERMS High impedance fault, mathematical morphology, distribution network.

I. INTRODUCTION

High Impedance Faults (HIFs) occur due to conductors contacting some surface with high impedance paths such as tree branches, concrete, asphalt road, etc. It is difficult to detect these types of faults with traditional overcurrent relays because the fault current in such faults is usually lower than what can be detected by the relays [1]. However, such faults, if not detected in time, can result in economic losses, fires, and safety hazards to the public. Currently, HIF is one of the key challenges in the protection system of distribution networks due to its complex nature and special features such as nonlinearity, asymmetry and periodicity. HIFs are often associated with arc events and occur at voltages lower than 25 kV, so the currents resulting from them are low, highly distorted, asymmetric, non-linear and alternating [2], [3]. These features overlap with other regular system phenomena such as capacitor switching, load switching, energizing the transformer, etc. (see [4] and [5]). Therefore, HIFs cannot be detected by typical relays.

In the last three decades, several methods have been presented for the detection of HIF. These methods can be generally classified into frequency domain algorithms [6], time domain algorithms [7], the combined frequency and time domain (hybrid) algorithms [8], and expert systems [9].

Frequency-based methods use sequence components (with their harmonics [6], [10]) and high frequency spectra [11]. Time domain algorithms include proportional control relays [7], stochastic numerical schemes [12], and signal superposition [13]. In the paradigm of hybrid methods,

The associate editor coordinating the review of this manuscript and approving it for publication was Tianhua Xu.

discrete wavelet transforms [4], [14], [15] has typically been proposed by researchers. Algorithms based on expert systems also use techniques such as Kalman filters [16], and training-based methods such as decision trees [17], artificial neural networks [18], [19], fuzzy neural methods and genetic schemes [20].

The typical characteristics of HIF currents such as nonlinearity, asymmetry and periodicity, have led researchers to use modern techniques such as artificial intelligence, wavelet transforms [21], [22] and the energy of wavelet coefficients for detection of HIF [23]. Most wavelet-based HIF detection approaches depend on complex reconstruction methods and require different decomposition levels based on the complexity of the original time series. In addition, the performance of wavelet-based methods is greatly affected by the choice of the mother wavelet, which can cause an increase in computational requirements.

A fast directional detection method based on zero sequence capacitance for HIF, LIF faults and transient states, is proposed in [24]. In [25], a two-level artificial neural network (ANN) is proposed for detecting HIFs based on synchronized current measurements. In [26], Kullback-Leibler divergence (KLD) is used to distinguish HIF from other disturbances and voltage swells/sags. In [27], a method based on the harmonic energy randomness index is proposed for detecting HIF. These methods have not consider the optimal micro-phase measurement unit (μPMU) placement. In [28], an HIF detection method using synchronized data divergence based on globally optimal μPMU placement, is proposed.

In [29], another HIF detection technique based on the observation of the distorted waveform and nonlinear current-voltage characteristics during the arc extinguishing process and its re-striking. In some methods [30], [31], the Tiger energy operator has been used for the detection of HIF. However, such techniques consider a large information window to confirm the occurrence of HIF. Due to the presence of special features in the current and voltage waveforms caused by high impedance faults, some researchers [32], [33] have used the mathematical morphology (MM) technique for signal processing and HIF detection.

When HIF occurs, there are many irregularities and changes in the waveform of current and voltage, and the MM technique can be used as a powerful tool to extract these changes for the purposes of HIF detection. In this paper, based on MM, an MGED is presented for HIF detection. The MGED is designed in such a way that it extracts edges and feathers of voltage signals. Based on these special features, an HIFDI scheme is introduced for the purposes of distinguishing and classifying HIF from other regular system phenomena. The proposed method is tested on the 20 kV test feeder and the IEEE 34-bus distribution test system simulated using EMTP.

The rest of the paper is organized as follows: The useful features of HIF and its model are explained in section II. Section III illustrate MM and the proposed MGED to detect edges of a signal. Feature extraction using MGED and the proposed algorithm for detecting HIF and other transient phenomena is described in section IV. The simulation results are outlined in section V. Finally, the conclusion is presented in section VI.

II. MODEL AND CHARACTERISTICS OF HIF

A. CHARACTERISTICS OF HIF

HIF is one of the disturbances of the power system, which prevents the production of the pickup currents of overcurrent relays, due to the high ground impedance associated with this fault type. HIFs usually occur in distribution networks (15-25 kV). HIFs are usually associated with the occurrence of an electric arc and have the following characteristics [3]:

☐ Discontinuity of the arc: in some cycles, the current is established due to the contact of the conductor, and in some cycles, the current is not established due to the interruption of the conductor contact.

☐ Current buildup and shoulder: the current amplitude gradually reaches its maximum and maintains a constant value for several cycles.

☐ Non-stationary Current: the frequency spectrum of the current changes with time.

☐ Randomness: both the amount of current, contact intervals and disconnection intervals of the conductor are random.

☐ Asymmetry: the fault current has different shapes and values in positive and negative half-cycles.

☐ Non-linear: The voltage-current characteristic of HIF is non-linear due to the presence of an arc.

☐ High frequency components in the current waveform: arcing leads to high frequency components in the current waveform.

B. HIF MODEL

HIFs are usually associated with an arc, which causes the fault current to be unpredictable and random. Depending on the type of surface involved in the fault path, the fault resistance may change due to the heat generated by the arc, randomly changing the amount of fault current. Therefore, HIF is a random phenomenon and leads to wide variations in amplitude, waveform and frequency content of current and voltage. Therefore, providing a suitable model for HIF that includes all the characteristics and behavior of HIF is not an easy task. So far, researchers have presented various models for HIF, although they are not complete, but because they are based on the results of practical experiments, they include the features of HIF to a large extent. The first HIF model with only one resistance at the fault location [34] and its more complete model including nonlinear impedances was presented in [35]. To show the asymmetric characteristic of the fault current, a model including two diodes and two DC voltage sources in reverse and parallel connection was presented in [36]. In subsequent research [37], the latter mentioned model was corrected by adding one (or two) variable resistors in series with DC voltage sources to model

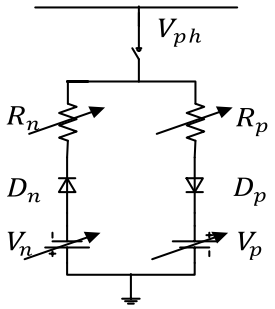

FIGURE 1. The proposed HIF model.

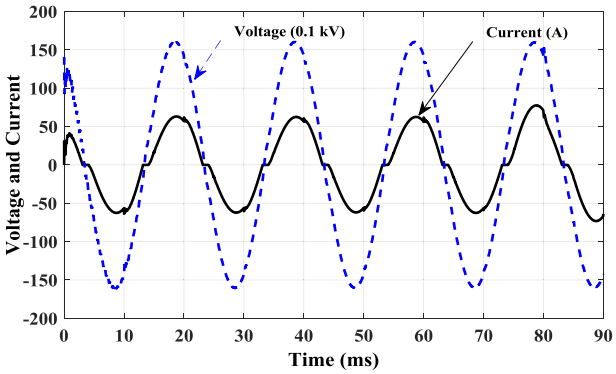

FIGURE 2. Voltage and current waveform for a typical HIF.

the random behavior of effective impedance and as a result of the randomness of the fault current. In other methods [18], differential equations have been used to model the behavior and characteristics of HIF.

In this paper, an HIF model including diode, variable DC voltage source and variable resistor (see Figure 1) is used [33]. This model contains almost all the characteristics of the fault current and includes two voltage sources (V_p and V_n) which are connected to two diodes (D_p and D_n) in series and reverse respectively. DC voltage sources do not have the same amplitude and output reacts randomly. This particular arrangement models the asymmetric nature of fault currents and intermediate arc outages. Two variable resistors are also connected in series with diodes. These resistances vary randomly and model the randomly varying arc resistance. The HIF model is placed between the phase with voltage V_{ph} and the ground. If $V_{ph} > V_p$, the fault current flows towards the ground, reversely if $V_{ph} < V_n$. For the condition when $V_n < V_{ph} < V_p$, no current will flow.

Considering the model described in Figure 1, the waveforms and the HIF voltage-current characteristic are shown in Figures 2 and 3, respectively. The latter mentioned results are similar to the experimental results obtained in [38]. According to Fig. 2, it is clear that the HIF current has nonlinear, asymmetric and random properties.

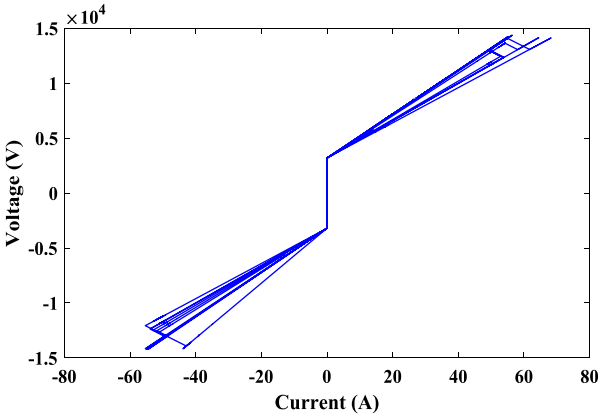

FIGURE 3. Voltage-current characteristic for a typical HIF.

III. PROPOSED MORPHOLGICAL GRADIENT EDGE DETECTOR (MGED)

A. EXTRACTING TRANSIENT CHARACTERISTICS OF A SIGNAL BY MM

Mathematical morphology (MM) was first introduced in 1964 by two French researchers named Matheron and Serra [39], [40]. MM can be defined as a theory and technique for analyzing spatial structures, based on set theory and integral geometry. This method is completely different from methods such as wavelet and Fourier transform, which are based on integral transformations, and as a nonlinear signal transform, it focuses on the shape and appearance of the signal in the time domain instead of the frequency domain. Dilation and Erosion are two primary and basic transformations in MM and all other transformations stem from these two components.

MM uses a function called Structuring Element (SE) for signal processing. The SE is the basis of all morphological transformations and is used as a probe to extract image and signal features. In terms of shape, the SE has different types, including linear, square, circular and other geometric shapes, of which the linear types should be used for signal processing. Assuming that f is a signal defined in the domain D_f and g is a SE defined in the domain D_g, the dilation and erosion of the signal $f(n)$ by $g(s)$ are defined by (1) and (2), respectively:

$$f_d(n) = (f \oplus g)(n) = \max\{f(n-s) + g(s)\} \quad |(n-s) \in D_f, s \in D_g \tag{1}$$

$$f_e(n) = (f \ominus g)(n) = \min\{f(n+s) - g(s)\} \quad |(n+s) \in D_f, s \in D_g. \tag{2}$$

where $f(n)$ is the main signal to be processed, $g(s)$ is the SE and $\oplus$ and $\ominus$ are erosion and dilation operators, respectively. Integers n and s are such that $n > s$. According to the characteristics of $f_d(n)$ and $f_e(n)$, the combination of these two operators can be used to detect the edges of a signal, which is explained in the next section.

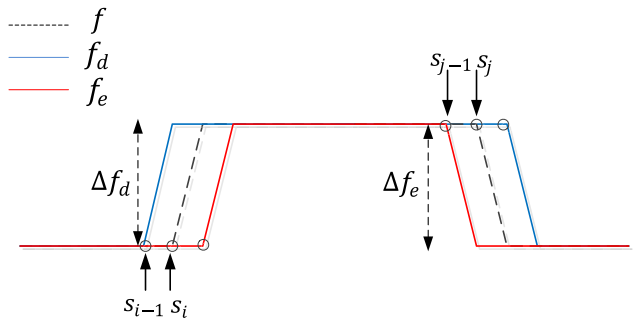

FIGURE 4. The effect of erosion and dilation operators on a signal sample at the ascending and descending edges. For ascending edge at sample s_i, $\Delta f_e = 0$, $\Delta f_d \neq 0$ and for descending edge at sample s_j, $\Delta f_d = 0$, $\Delta f_e \neq 0$.

B. SIGNAL EDGE DETECTION BASED ON MORPHOLOGICAL GRADIENT (MG)

MG is defined as the difference between dilation and erosion of a signal by SE. By selecting a flat SE, MG can be used as a powerful tool for signal edge detection. Figure 4 shows the processing of a sample signal, with ascending and descending edges, by dilation and erosion operators. According to the figure, it is clear that when there is no change in the signal, the f_d and f_e operators match and are in phase, but when the signal changes, they are out of phase with each other. In other words, for an ascending edge, the dilation signal lags the erosion signal, and for a descending edge, leads the erosion signal. These characteristic can be used for signal edge detection. According to Figure 4, for the s_i th sample of signal f as an ascending edge

$$\Delta f_d - \Delta f_e = (f_d(s_i) - f_d(s_{i-1})) - (f_e(s_i) - f_e(s_{i-1})) > \delta. \quad (3)$$

where δ is the threshold and has a very small positive value. In this paper, its value is considered to be 0.0001. It is clear that for ascending edge that $\Delta f_e = 0$. Similarly, for the $s_j th$ sample of signal f as a descending edge

$$\Delta f_e - \Delta f_d = (f_e(s_j) - f_e(s_{j-1})) - (f_d(s_j) - f_d(s_{j-1})) < -\delta. \quad (4)$$

According to Figure 4, it is clear that for descending edge $\Delta f_d = 0$. Therefore, the set of samples of ascending and descending edges in signal f can be defined as

$$E^{\uparrow} = \{s_i \in f | (\Delta f_d - \Delta f_e) > \delta \quad (5)$$

$$E^{\downarrow} = \{s_j \in f | (\Delta f_e - \Delta f_d) < -\delta. \quad (6)$$

where $E^{\uparrow}$ and $E^{\downarrow}$ are the set of samples of ascending and descending edges in signal f, respectively. According to equation (1) to (6), MGED for signal f can be defined as a digital quantity in the following manner:

$$\text{MGED}_f = \begin{cases} 1 \; \forall s_i \in E^{\uparrow}, & s_j \in E^{\downarrow} i, j = 1, 2, \ldots, N \\ 0 & \text{other} \end{cases} \quad (7)$$

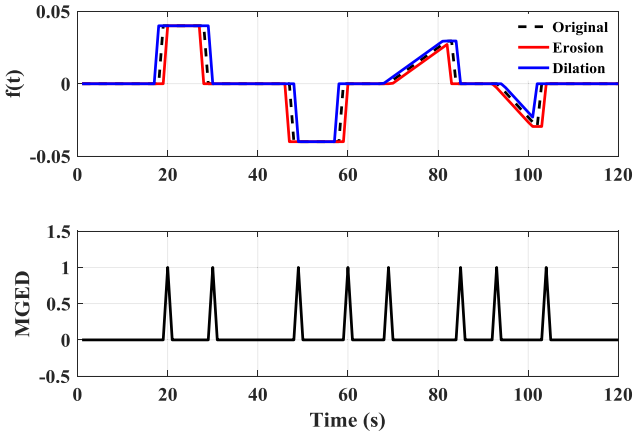

FIGURE 5. Sample signal f and its processing with MGED. For times when the signal f changes (ascending and descending edges), the MGED output is 1, and for times when the signal is not changing, the MGED output is 0.

According to equation (7), MGED has a non-zero output only for edges or changes in the signal, therefore, it can be defined as a digital quantity whose output has only "1" and "0" values. The value "1" is for signal samples that act as edges or changes in the signal, and the value "0" is for other signal samples. In Figure 5, a sample signal f (with step and ramp changes) and its processing with MGED is shown. According to the figure, it can be seen that the MGED accurately and clearly detects changes or edges of the signal.

C. REDUCE THE EFFECT OF NOISE

Transient signals in the power system usually have noise, which can have a negative effect on MGED performance. To reduce the effect of noise in signals, a morphological filter is introduced in this section. First, two opening ($\circ$) and closing ($\bullet$) operators, which are obtained from the combination of dilation and erosion operators, are defined as follows:

$$(f \circ g)(n) = ((f \ominus g) \oplus g)(n) \quad (8)$$

$$(f \bullet g)(n) = ((f \oplus g)g)(n) \quad (9)$$

where $f \circ g$ and fg are the opening and closing of the signal f by the g as the SE, respectively. Opening and closing operators are very effective in reducing the noise of power system signals. By combining these two operators, the open-close and close-open (OCCO) filter [41], [42] is ultimately defined as

$$\text{OCCO}(n) = f(n) \bullet [f(n) \circ g(s)] + f(n) \circ [f(n) \bullet g(s)] \quad (10)$$

It is found that the OCCO filter is able to eliminate the majority of the noise associated with typical transient signals [41]. Therefore, the OCCO filter is used in this paper.

IV. FEATURE EXTRACTION USING PROPOSED MGED

The main goal is to distinguish HIFs from other disturbances in the network. Therefore, according to the MG, these

disturbances include capacitor switching, load switching, transformer inrush current and CT saturation. These mentioned characteristics depend on the shape of the current or voltage waveform. For this purpose, all disturbances have been simulated in this paper, and then by processing and analyzing their waveforms, the features of each have been extracted using the MGED method. Finally, according to these extracted features, we propose a new simple index to distinguish a HIF from other regular system phenomena.

A. HIF FEATURES EXTRACTION USING MGED

Figure 6 shows the voltage waveform for a phase A to ground HIF at 30 ms and the corresponding MGED output. Enlarged parts of the MGED output are inserted to clearly show the edges. According to the figure, it is clear that before the fault occurs, the MGED output is zero for the normal state, but when the fault occurs, there are changes in the voltage signal and as a result, many edges occur for a long period of time in the first and second cycles (parts I and II) and these changes are well reflected in the output of MGED.

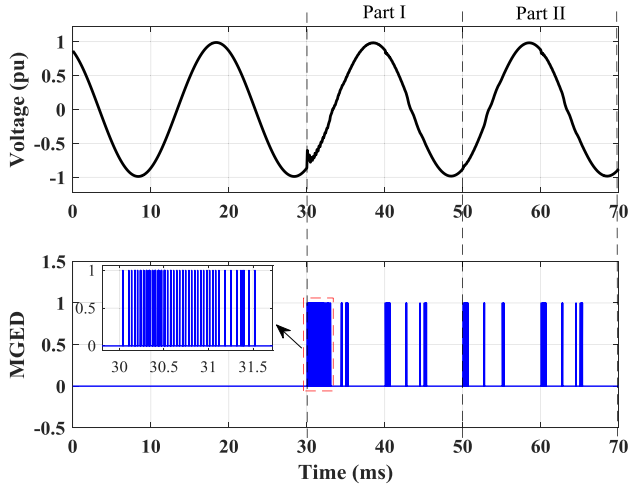

FIGURE 6. Voltage waveform for a phase A to ground HIF at 30 ms together with the MGED output.

B. CAPACITOR SWITCHING FEATURES EXTRACTION USING MGED

The act of switching to connect or disconnect a capacitor bank leads to transient states in current and voltage waveforms. These transient states are intense at the first moment of switching and usually decay after a short period of time. Figure 7 shows the waveform of the current during capacitor switching at 30 ms and the corresponding MGED output. According to the figure, it can be seen that in capacitor switching, the duration of the transient state created is less than in HIF mode, and the effect of capacitor switching on voltage and current waveforms disappears after a short period of time (a fraction of a cycle). Therefore, the changes in the voltage signal and edges according to MGED output are seen only in the first cycle (part I).

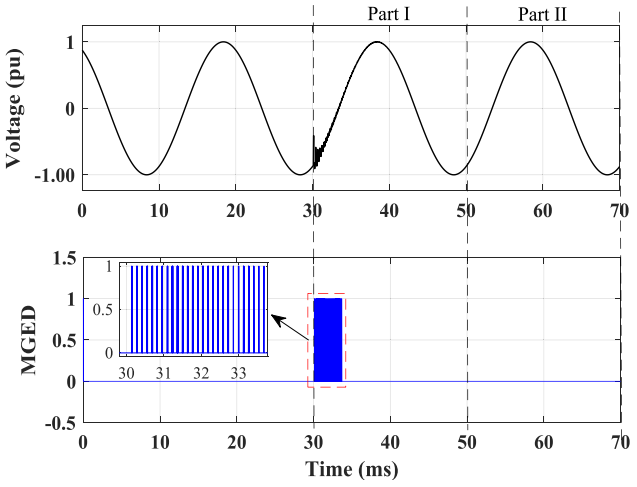

FIGURE 7. Voltage waveform and MGED output for capacitor switching at 30 ms.

C. LOAD SWITCHING FEATURES EXTRACTION USING MGED

Load switching causes frequency changes and transient states in a short period of time in the waveform of voltage and current. Figure 8 shows the voltage waveform for the load switching mode and the corresponding MGED output. According to the figure, it is clear that in this case too, changes in the signal and transient states occur in a short period of time, and the output of MGED has a small number of edges that appear only in the first cycle (part I) which is different from the HIF.

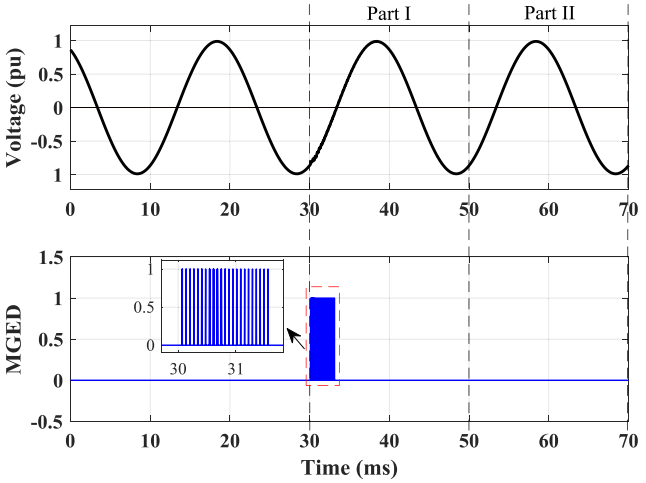

FIGURE 8. Voltage waveform and MGED output for load switching at 30 ms.

D. CT SATURATION FEATURES EXTRACTION USING MGED

The operation of switching to energize a transformer creates a large transient current (inrush current). The DC offset during transformer energization/inrush causes DC saturation. Severity of saturation depends on the switching instant. Deep saturation occurs in zero – voltage switching.

In the DC saturation, the current waveform in the secondary side of CT is distorted, and this distortion

takes a few cycles alternately and asymmetrically. Figure 9 shows the voltage waveforms for the DC saturation and the corresponding MGED output. According to the figure, it can be seen that after the first few cycles, saturation occurs in the core and distortions appear in the secondary waveform. Another CT saturation mode occurs due to high short circuit current in the primary, which is called AC saturation. In this case, the distortion created in the secondary waveform is symmetrical and alternating. Figure 10 shows the current and voltage waveforms for the AC saturation and the corresponding MGED output. According to the figure, it is clear that in the CT saturation mode, unlike other disturbances, that the transient changes created are small, intermittent and equal in all cycles after the disturbance.

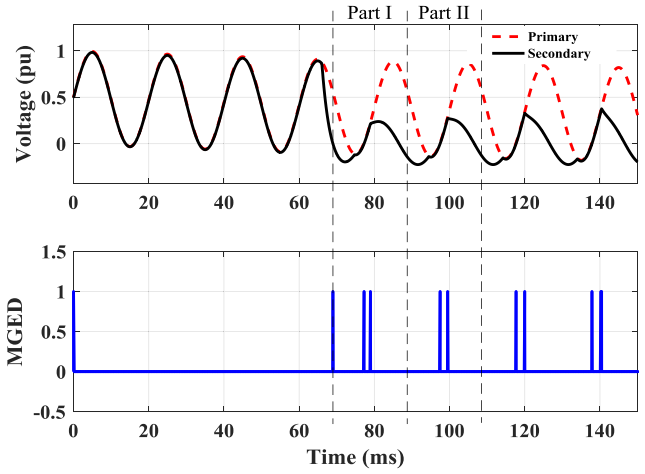

FIGURE 9. Voltage waveform and MGED output for CT saturation caused by inrush current (DC saturation).

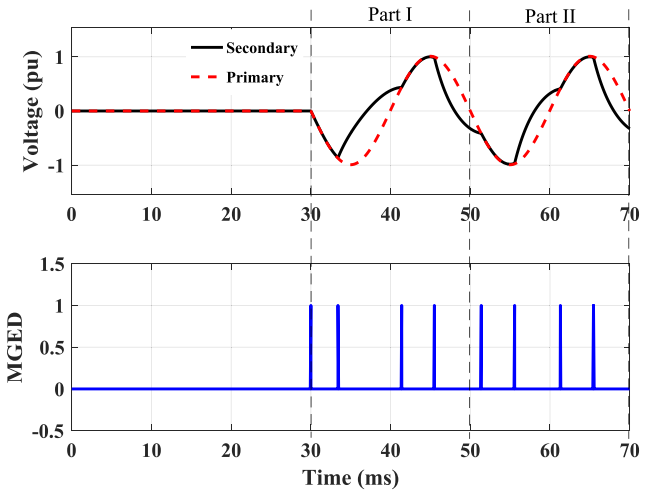

FIGURE 10. Voltage waveform and MGED output for CT saturation caused by short circuit current (AC saturation).

E. PROPOSED HIF DETECTION ALGORITHM

According to the extracted properties of HIF, the studied phenomena using MGED method and the difference of MGED output related to HIF with other regular system phenomena, it is possible to distinguish HIF from other disturbances. According to Figures 6 to 10, if we denote the number of edges in the first and second cycles of the signal f after the moment of the fault starting as NE_1 and NE_2 respectively, then:

$$NE_1 = \sum_{i=i_0}^{i_0+n} \mathrm{MGED}_f(s_i) \tag{11}$$

$$NE_2 = \sum_{i=i_0+n}^{i_0+2n} \mathrm{MGED}_f(s_i)\,. \tag{12}$$

where n is the number of samples in one cycle and i_0 is the first sample corresponding to the start of the disturbance. According to Figures 6 to 10, in the capacitor and load switching, there are some edges or changes in the signal only in the first quarter of the first cycle or a part of the first cycle, that is; $E_2 = 0$ and $E_1 \neq 0$. For HIF, the edges exist in a long period of time and in all cycles, and the number of edges in the first cycle is more than other cycles. i.e. if $E_1 > E_2$. The waveform of CT saturation is different from other disturbances. In this case, there are less transient changes in the signal and these changes are repeated alternately and equally in the first and second cycles. In other words, the number of edges is limited and they are equal in the first, second and third cycles, that is when $E_1 = E_2$. Therefore, by defining the *HIFDI*, it is possible to distinguish the HIF fault from other disturbances:

$$HIFDI = \frac{NE_1 - NE_2}{NE_1 + NE_2} \tag{13}$$

According to the mentioned features for each of the disturbances, it is clear that in the case of capacitor and load switching, that $HIFDI = 1$, in CT saturation mode, $HIFDI = 0$ and for HIF mode, it is always $0 < HIFDI < 1$. The flowchart of the proposed method for detecting HIF from other disturbances is shown in Figure 11. According to the proposed algorithm, by sampling the voltage signal and processing it with MGED, if the output of MGED is zero, the network is in normal condition, otherwise, the type of disturbances including capacitor or load switching, CT saturation and HIF is detected.

V. SIMULATION RESULTS

A. 20 KV DISTRIBUTION FEEDER

In this section, to illustrate the performance of the proposed method, a sample of 20 kV distribution feeder with a single line diagram shown in Figure 12, is simulated in EMTP and some of the results are presented. The length of the feeder is 20 km and the location of the HIF fault is considered 10 km away from the bus M where the measuring devices are installed. Other disturbances such as capacitor switching (ON and OFF), load switching (ON and OFF) and CT saturation mode have also been simulated. After each simulation, voltage and current time series are transferred to MATLAB software for analysis, processing with MGED and

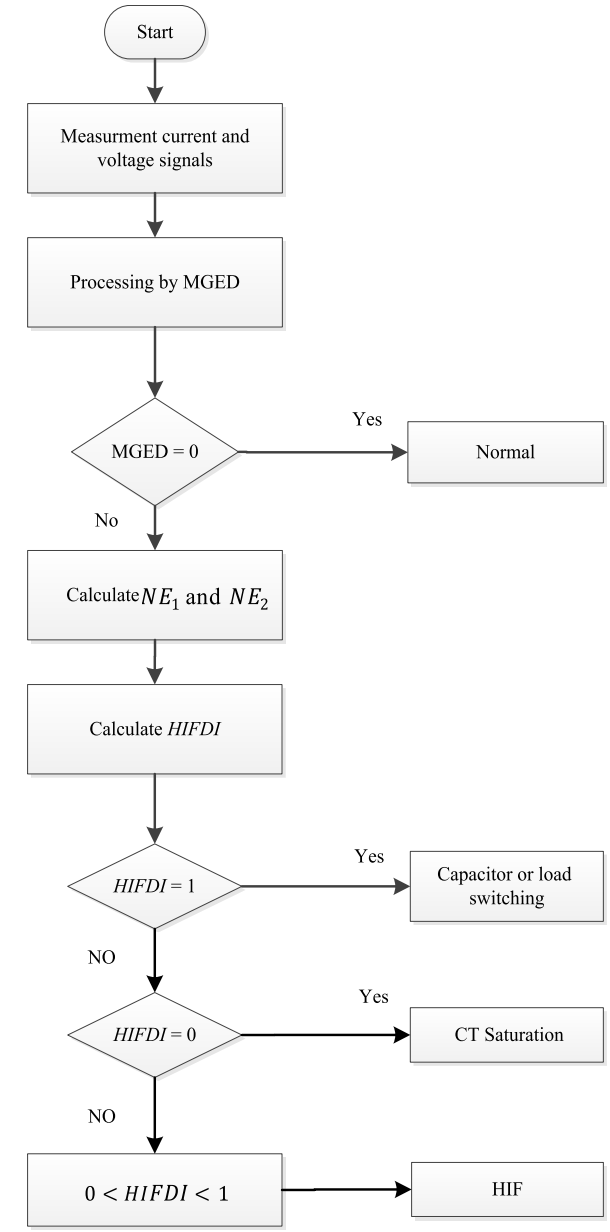

FIGURE 11. Flowchart of the proposed method for HIF detection.

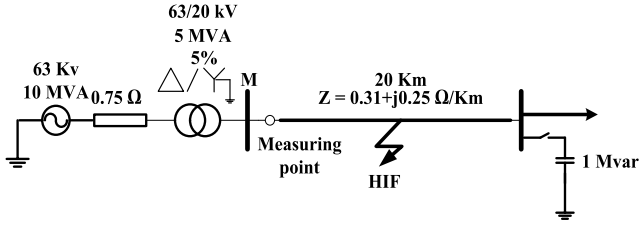

FIGURE 12. Single line diagram of the simulated distribution feeder.

the execution of the proposed algorithm. For different HIFs on phases A, B and C, as well as for capacitor switching, load switching and CT saturation, simulations are done and the results are shown in Table 1.

TABLE 1. The result of applying the proposed HIF detection method for different fault conditions (20 kV distribution feeder).

Fault type	Inception time	NE_1	NE_2	$HIFDI$
HIF				
A	35	124	40	0.512
A	40	98	32	0.507
A	45	112	37	0.503
A	50	87	19	0.641
B	35	95	27	0.557
B	40	118	39	0.503
B	45	92	24	0.586
B	50	107	33	0.528
C	35	103	19	0.688
C	40	96	25	0.581
C	45	117	38	0.509
C	50	89	21	0.618
Capacitor switching				
ABC	35	94	0	1
ABC	40	83	0	1
ABC	45	58	0	1
ABC	50	89	0	1
A	35	43	0	1
A	40	38	0	1
B	45	47	0	1
C	50	34	0	1
C(OFF)	35	3	0	1
ABC(OFF)	40	12	0	1
ABC(OFF)	45	9	0	1
Load switching				
ABC	35	36	0	1
ABC	40	42	0	1
ABC	45	33	0	1
ABC	50	42	0	1
A	35	26	0	1
B	40	32	0	1
C	50	29	0	1
ABC (OFF)	35	2	0	1
ABC (OFF)	40	3	0	1
CT saturation				
AC saturation	35	4	4	0
AC saturation	40	4	4	0
AC saturation	50	4	4	0
DC saturation	35	3	3	0
DC saturation	40	3	3	0
DC saturation	50	3	3	0

For each mode, parameters NE_1, NE_2 and $HIFDI$ are calculated and shown in Table 1. In order to better evaluate

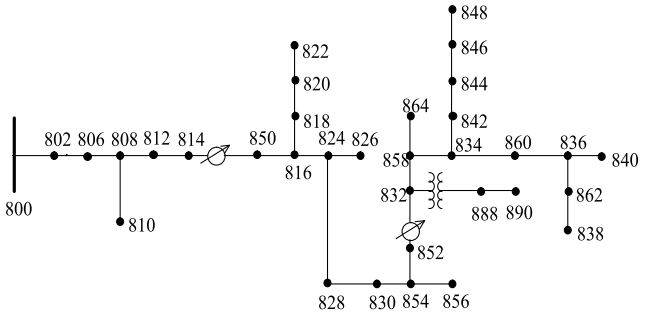

FIGURE 13. IEEE 34-node test feeder.

the performance of the proposed method, different times of a cycle for the start of a fault or disturbance have been considered from 35 to 50 ms because the intensity of the transient state created in the voltage waveform depends on the time of the start of the fault or disturbance. The results of the table show that for the HIF, there are transient changes in the voltage waveform over a long period of time, and as a result, parameters E_1 and E_2 have non-zero values, but in the capacitor and load switching, transient changes in the waveform appear in a short period of time (the first quarter of the cycle), hence only parameter E_1 has non-zero values and parameter E_2 has zero value. Therefore, the value of *HIFDI* for capacitor and load switching is always equal to 1.

CT saturation waveforms are completely different from other disturbances. Two AC and DC modes have been investigated for CT saturation. In AC saturation mode, which occurs due to high current caused by short circuit, the CT core goes into saturation and causes distortion in the secondary side of CT, which appears symmetrically and alternately in the waveform. In the DC saturation mode caused by the inrush current of the transformer, the distortions are created asymmetrically and alternately in the secondary side of CT as shown in Figure 9. Therefore, in the CT saturation mode in the form of AC or DC, $HIFDI = 0$.

As the results show, the proposed algorithm is able to distinguish all HIF modes from other disturbances and with high accuracy. Also to some benefit, the proposed method detects HIF in a short period of time (two cycles at a frequency of 50 Hz) equivalent to 40 milliseconds.

B. IEEE 34-NODE TEST FEEDER

To better evaluate the effectiveness of the proposed method, the IEEE 34-node feeder, with a single-line diagram as shown in Figure 13, was studied and simulated. The network consists of five three-phase and single-phase overhead lines with different conductors, simulated in EMTP with a frequency-dependent model. Network loads are also three-phase and single-phase loads. A six-pulse rectifier load is considered at node 830, which represents a non-linear and harmonic load. The network is connected to the distribution station using a distribution transformer 25 KVA, 69/24.9 kV. Full information of this network is presented in [33].

Different locations of HIF, capacitor switching, CT saturation, linear and non-linear load switching at nodes 816, 830, 834, 840, 844, 848 and 890 at different times from 20 to 60 ms (different inception angles) were considered. By varying parameters such as residual flux, initial current amplitude, and fault inception angle, different waveforms for CT saturation state were obtained and studied. The nonlinear loads are DC loads connected at nodes 840 and 848 via a six-pulse converter. The fire angle of thyristors varies from 5 to 50 degrees and their power factor varies from 0.7 to 0.95. Voltage and current signal processing and measuring devices have been placed at the transformer station (node 800).

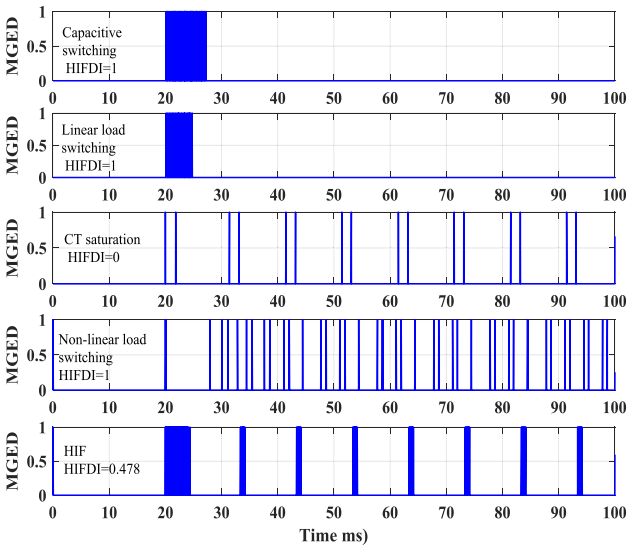

FIGURE 14. MGED output for capacitor switching, linear load switching, CT saturation, non-linear load switching and HIF (fault inception time = 20 ms) IEEE 34-node feeder.

A summary of the simulation results for different fault conditions is presented in Table 2. These results show that the proposed method can distinguish HIF from other network disturbances. Figure 14 shows the MGED output for HIE at node 816, load switching at node 840, capacitive and nonlinear load switching at node 848 and CT saturation at node 816. For all these situations, the fault inception time is considered at 20 ms. From Figure 14, it is clear that in the case of capacitor and linear load switching, transient changes in the signal are visible only during the first cycle and hence the MGED filter has only non-zero value in the first cycle.

For the HIF, nonlinear load switching and CT saturation cases, transient changes continue in the second and subsequent cycles, and thus the MGED filter has a non-zero value during these cycles. However, the transient changes in the nonlinear load switching and CT saturation cases are similar in successive cycles, i.e. $NE_1 = NE_2$. Therefore, the *HIFDI* for these conditions becomes zero.

C. COMPARISON

In this section, the performance of the proposed method is compared with other existing methods [33] and [43] based on mathematical morphology. In [43], the voltage signal is processed by morphology and then the energy index is used

TABLE 2. The result of applying the proposed HIF detection method for different fault conditions (IEEE 34-node feeder).

Fault type	Inception time	NE_1	NE_2	$HIFDI$
HIF				
A	35	156	64	0.418
A	40	147	57	0.441
B	45	138	51	0.460
B	50	141	52	0.461
C	35	123	41	0.5
C	40	101	35	0.485
Capacitor switching				
ABC (ON)	35	120	0	1
ABC (ON)	40	113	0	1
ABC (OFF)	45	98	0	1
ABC (OFF)	50	96	0	1
Linear Load switching				
ABC (ON)	35	82	0	1
ABC (ON)	40	77	0	1
ABC (OFF)	45	65	0	1
ABC (OFF)	50	69	0	1
Non-linear Load Switching				
B	40	41	0	1
C	50	37	0	1
ABC (OFF)	35	9	0	1
ABC (OFF)	40	11	0	1
CT saturation				
AC saturation	35	4	4	0
AC saturation	40	4	4	0
AC saturation	50	4	4	0
DC saturation	35	3	3	0
DC saturation	40	3	3	0
DC saturation	50	3	3	0

for diagnosis. According to this method, if the index value is above the threshold for a period greater than 80 ms, it is diagnosed as a HIF, and for a period less than 80 ms, it is diagnosed as a load or capacitor switching.

In [33], Closing Opening Difference Operation (CODO) as a morphological transformation is also used for signal processing. According to this method, the CODO output for normal conditions is zero, but for fault and switching conditions, it has a non-zero output in the form of spikes with different amplitudes. If the output exceeds the threshold within the given time then it is diagnosed as a HIF, otherwise it is diagnosed as a load or capacitor switching.

The method proposed in this paper uses a MGED filter to process the signal. This filter is designed so that its output is zero or one and by deploying this method, the number of signal edges is determined. The comparison of the above methods with the proposed method are presented in

TABLE 3. Comparing the proposed method with other related methods.

Method	Technique	HIF	Capacitor switching	Load switching	CT saturation	Detection time (ms)
[33]	CODO filter-Threshold time	✓	✓	✓	×	80
[43]	Energy - index Threshold time	✓	✓	✓	×	588
Proposed method	MGED-Number of edges	✓	✓	✓	✓	40

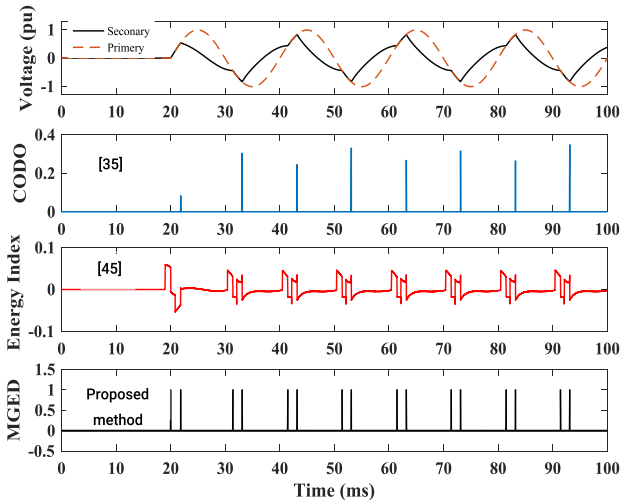

FIGURE 15. Comparison of the performance of the proposed method with [33] and [43] in CT saturation state.

Table 3. According to this table, the reference methods are not capable of detecting HIF in all cases. The effectiveness of these methods on CT saturation has not been studied. The simulation results of the CT saturation state, according to Figure 15, show that these methods are not capable of detecting the CT saturation phenomenon because the OCDO output (in method [33]) and the energy index (in method [43]) over a long period of time and beyond a certain time period (threshold) are non-zero, corresponding to an HIF. However, the algorithm proposed in the paper operates based on the number of edges in the first and second cycles after a fault occurs, ultimately detecting the CT saturation phenomenon with certainty. Furthermore, the proposed method detects HIF after two cycles equivalent to 40 ms with a frequency of 50 Hz. while method [43] detects faults after 80 ms and method [33] detects faultsafter 588 ms in certain number of conditions. In other words, the proposed method has a higher detection speed.

VI. CONCLUSION

In this paper, a new scheme based on MM for HIF detection in distribution network was presented. In the proposed method, by sampling the voltage signals close to the substation and processing them with MGED, a suitable detection

index *HIFDI* is defined and based on this index, HIF fault and other disturbances such as capacitor switching (ON and OFF), Load switching (ON and OFF), CT saturation and transformer inrush current are detected. The novelty of the proposed method lies in it only uses two cycles after the fault inception time to detect the fault.

Since the proposed method uses the MM technique, which only has addition and subtraction operators, for signal processing, it has a lower computational burden, higher speed and accuracy than other methods. Various simulations for different conditions including types of faults and disturbances with different inception times were performed in the EMTP software environment. The compared results show that the proposed method can detect HIF successfully and with high accuracy.

REFERENCES

[1] J. Tengdin, R. Westfall, and K. Stephan, "High impedance fault detection technology," PSRC Working Group D15, Inst. Elect. Electron. Eng. (IEEE), USA, Tech. Rep. 15, 1996.

[2] S. R. Nam, J. K. Park, Y. C. Kang, and T. H. Kim, "A modeling method of a high impedance fault in a distribution system using two series time-varying resistances in EMTP," *IEEE Trans. Power Del.*, vol. 3, no. 4, pp. 1175–1180, Oct. 2001.

[3] A. Aljohani and I. Habiballah, "High-impedance fault diagnosis: A review," *Energies*, vol. 13, no. 23, p. 6447, Dec. 2020.

[4] T. M. Lai, L. A. Snider, E. Lo, and D. Sutanto, "High-impedance fault detection using discrete wavelet transform and frequency range and RMS conversion," *IEEE Trans. Power Del.*, vol. 20, no. 1, pp. 397–407, Jan. 2005.

[5] M. Sarlak and S. M. Shahrtash, "SVM-based method for high-impedance faults detection in distribution networks," *COMPEL-Int. J. Comput. Math. Electr. Electron. Eng.*, vol. 30, no. 2, pp. 431–450, Mar. 2011.

[6] K.-Y. Lien, S.-L. Chen, C.-J. Liao, T.-Y. Guo, T.-M. Lin, and J.-S. Shen, "Energy variance criterion and threshold tuning scheme for high impedance fault detection," *IEEE Trans. Power Del.*, vol. 14, no. 3, pp. 810–817, Jul. 1999.

[7] J. Carr, "Detection of high impedance faults on multi-grounded primary distribution systems," *IEEE Power Eng. Rev.*, vol. PER-1, no. 4, pp. 69–70, Apr. 1981.

[8] A.-R. Sedighi, M.-R. Haghifam, O. P. Malik, and M.-H. Ghassemian, "High impedance fault detection based on wavelet transform and statistical pattern recognition," *IEEE Trans. Power Del.*, vol. 20, no. 4, pp. 2414–2421, Oct. 2005.

[9] S. Sarangi, B. K. Sahu, and P. K. Rout, "High-impedance fault identification and location by using mode decomposition integrated adaptive multi-kernel extreme learning machine technique for distributed generator-based microgrid," *Electr. Eng.*, vol. 105, no. 1, pp. 383–406, Feb. 2023.

[10] G. N. Lopes, T. S. Menezes, G. G. Santos, L. H. P. C. Trondoli, and J. C. M. Vieira, "High impedance fault detection based on harmonic energy variation via S-transform," *Int. J. Electr. Power Energy Syst.*, vol. 136, Mar. 2022, Art. no. 107681.

[11] B. M. Aucoin and B. D. Russell, "Distribution high-impedance fault detection using high-frequency current components," *IEEE Trans. Power App. Syst.*, vol. PAS-101, no. 6, pp. 1596–1606, Jun. 1982.

[12] C. Benner, P. Carswell, and B. Don Russell, "Improved algorithm for detecting arcing faults using random fault behavior," *Electr. Power Syst. Res.*, vol. 17, no. 1, pp. 49–56, Jul. 1989.

[13] I. Zamora, A. J. Mazon, K. J. Sagastabeitia, and J. J. Zamora, "New method for detecting low current faults in electrical distribution systems," *IEEE Trans. Power Del.*, vol. 22, no. 4, pp. 2072–2079, Oct. 2007.

[14] S. Lavanya, S. Prabakaran, and N. A. Kumar, "Analysis of high impedance fault using discrete wavelet transform technique," *Int. J. Eng. Trends Technol.*, vol. 70, no. 8, pp. 238–246, Aug. 2022.

[15] E. C. M. Maritz, J. M. Maritz, and M. Salehi, "A travelling wave-based fault location strategy using the concepts of metric dimension and vertex covers in a graph," *IEEE Access*, vol. 9, pp. 155815–155825, 2021.

[16] A. A. Girgis, W. Chang, and E. B. Makram, "Analysis of high-impedance fault generated signals using a Kalman filtering approach," *IEEE Trans. Power Del.*, vol. 5, no. 4, pp. 1714–1724, 1990.

[17] Y. Sheng and S. M. Rovnyak, "Decision tree-based methodology for high impedance fault detection," *IEEE Trans. Power Del.*, vol. 19, no. 2, pp. 533–536, Apr. 2004.

[18] J. G. S. Carvalho, A. R. Almeida, D. D. Ferreira, B. F. dos Santos, L. H. P. Vasconcelos, and D. de Oliveira Sobreira, "High-impedance fault modeling and classification in power distribution networks," *Electric Power Syst. Res.*, vol. 204, Mar. 2022, Art. no. 107676.

[19] A. H. Etemadi and M. Sanaye-Pasand, "High-impedance fault detection using multi-resolution signal decomposition and adaptive neural fuzzy inference system," *IET Gener., Transmiss. Distrib.*, vol. 2, no. 1, p. 110, 2008.

[20] M.-R. Haghifam, A.-R. Sedighi, and O. P. Malik, "Development of a fuzzy inference system based on genetic algorithm for high-impedance fault detection," *IEE Proc.-Gener., Transmiss. Distrib.*, vol. 153, no. 3, p. 359, 2006.

[21] L. Peretto, R. Sasdelli, and R. Tinarelli, "On uncertainty in wavelet based signal analysis," *IEEE Trans. Instrum. Meas.*, vol. 54, no. 4, pp. 1593–1599, Jul. 2005.

[22] M. Sarlak and S. M. Shahrtash, "High-impedance faulted branch identification using magnetic-field signature analysis," *IEEE Trans. Power Del.*, vol. 28, no. 1, pp. 67–74, Jan. 2013.

[23] F. B. Costa, "Fault-induced transient detection based on real-time analysis of the wavelet coefficient energy," *IEEE Trans. Power Del.*, vol. 29, no. 1, pp. 140–153, Feb. 2014.

[24] C. Gonzalez, J. Tant, J. G. Germain, T. De Rybel, and J. Driesen, "Directional, high-impedance fault detection in isolated neutral distribution grids," *IEEE Trans. Power Del.*, vol. 33, no. 5, pp. 2474–2483, Oct. 2018.

[25] J. J. G. Ledesma, K. B. do Nascimento, L. R. de Araujo, and D. R. R. Penido, "A two-level ANN-based method using synchronized measurements to locate high-impedance fault in distribution systems," *Electr. Power Syst. Res.*, vol. 188, Nov. 2020, Art. no. 106576.

[26] S. Nezamzadeh-Ejieh and I. Sadeghkhani, "HIF detection in distribution networks based on Kullback–Leibler divergence," *IET Gener., Transmiss. Distrib.*, vol. 14, no. 1, pp. 29–36, Jan. 2020.

[27] M. Wei, F. Shi, H. Zhang, Z. Jin, V. Terzija, J. Zhou, and H. Bao, "High impedance arc fault detection based on the harmonic randomness and waveform distortion in the distribution system," *IEEE Trans. Power Del.*, vol. 35, no. 2, pp. 837–850, Apr. 2020.

[28] Y. Liu, Y. Zhao, L. Wang, C. Fang, B. Xie, and L. Cui, "High-impedance fault detection method based on feature extraction and synchronous data divergence discrimination in distribution networks," *J. Modern Power Syst. Clean Energy*, vol. 11, no. 4, pp. 1235–1246, Jul. 2023.

[29] B. Wang, J. Geng, and X. Dong, "High-impedance fault detection based on nonlinear voltage–current characteristic profile identification," *IEEE Trans. Smart Grid*, vol. 9, no. 4, pp. 3783–3791, Jul. 2018.

[30] X. Wang, J. Gao, X. Wei, G. Song, L. Wu, J. Liu, Z. Zeng, and M. Kheshti, "High impedance fault detection method based on variational mode decomposition and Teager–Kaiser energy operators for distribution network," *IEEE Trans. Smart Grid*, vol. 10, no. 6, pp. 6041–6054, Nov. 2019.

[31] M. Biswal, S. Ghore, O. P. Malik, and R. C. Bansal, "Development of time-frequency based approach to detect high impedance fault in an inverter interfaced distribution system," *IEEE Trans. Power Del.*, vol. 36, no. 6, pp. 3825–3833, Dec. 2021.

[32] M. Sarlak and S. M. Shahrtash, "High impedance fault detection using combination of multi-layer perceptron neural networks based on multi-resolution morphological gradient features of current waveform," *IET Gener., Transmiss. Distrib.*, vol. 5, no. 5, p. 588, 2011.

[33] S. Gautam and S. M. Brahma, "Detection of high impedance fault in power distribution systems using mathematical morphology," *IEEE Trans. Power Syst.*, vol. 28, no. 2, pp. 1226–1234, May 2013.

[34] R. E. Lee and M. T. Bishop, "A comparison of measured high impedance fault data to digital computer modeling results," *IEEE Power Eng. Rev.*, vol. PER-5, no. 10, pp. 35–36, Oct. 1985.

[35] D. C. Yu and S. H. Khan, "An adaptive high and low impedance fault detection method," *IEEE Trans. Power Del.*, vol. 9, no. 4, pp. 1812–1821, Oct. 1994.

[36] A. E. Emanuel, D. Cyganski, J. A. Orr, S. Shiller, and E. M. Gulachenski, "High impedance fault arcing on Sandy soil in 15 kV distribution feeders: Contributions to the evaluation of the low frequency spectrum," *IEEE Trans. Power Del.*, vol. 5, no. 2, pp. 676–686, Apr. 1990.
[37] E. Sortomme, S. S. Venkata, and J. Mitra, "Microgrid protection using communication-assisted digital relays," *IEEE Trans. Power Del.*, vol. 25, no. 4, pp. 2789–2796, Oct. 2010.
[38] N. Elkalashy, M. Lehtonen, H. Darwish, M. Izzularab, and A.-M. Taalab, "Modeling and experimental verification of high impedance arcing fault in medium voltage networks," *IEEE Trans. Dielectr. Electr. Insul.*, vol. 14, no. 2, pp. 375–383, Apr. 2007.
[39] G. Matheron, *Random Sets and Integral Geometry*. New York, NY, USA: Wiley, 1975.
[40] J. Serra, *Image Analysis and Mathematical Morphology*. New York, NY, USA: Academic, 1982.
[41] F. Namdari and M. Salehi, "High-speed protection scheme based on initial current traveling wave for transmission lines employing mathematical morphology," *IEEE Trans. Power Del.*, vol. 32, no. 1, pp. 246–253, Feb. 2017.
[42] M. Salehi and F. Namdari, "Fault classification and faulted phase selection for transmission line using morphological edge detection filter," *IET Gener., Transmiss. Distrib.*, vol. 12, no. 7, pp. 1595–1605, Apr. 2018.
[43] R. R. Panigrahi, M. Mishra, A. Rajan, and S. Mohapatra, "High impedance fault detection based on mathematical morphology for radial distribution network," in *Proc. Int. Conf. Appl. Electromagn., Signal Process. Commun. (AESPC)*, Bhubaneswar, India, Oct. 2018, pp. 1–6.

MOSLEM SALEHI was born in Alaeshtar, Lorestan, Iran, in 1980. He received the B.Sc. and M.Sc. degrees in electrical engineering from Shahid Rajaee Teacher Training University, Tehran, Iran, in 2003 and 2011, respectively, and Ph.D. degree in electrical engineering from Lorestan University, Khorramabad, Iran, in 2018. Since 2019, he has been a Lecturer in electrical engineering with Technical and Vocational University (TVU). His research interests include power system protection, power system transient, fault location, digital protective relays, and application of artificial intelligence in power systems.

MAHDI ZOLFAGHARI (Member, IEEE) was born in Aleshtar, Lorestan, Iran, in 1987. He received the Ph.D. degree (Hons.) in electrical power engineering from the Department of Electrical Engineering, Amirkabir University of Technology (AUT, formerly, Tehran Polytechnic), Tehran, Iran, in 2019. From 2019 to 2020, he worked as a Post-doctoral Research Fellow at AUT with the support of Elite National Foundation of Iran. In 2021, he joined the Power System Dynamic and Stability Studies Research Group at Iran Grid Management Company (IGMC), Tehran, and at the same time, he has been working as an Adjunct Research Professor with the Power System Secure Operation Research Center, AUT. He has authored or coauthored seven technical books and more than 40 papers. His research interests include smart grids, renewable integrated power systems, model estimation, analysis and robust control of complex and uncertain systems. He is a member of the Iranian Inventors Association. He also acts as an Editor for the *Journal of Advanced Research in Electrical and Electronics Engineering*, Australia.

JACQUES M. MARITZ received the master's and Ph.D. degrees in astrophysics from the University of the Free State, South Africa, in 2017. Since 2017, he has been a Lecturer in engineering sciences with the University of the Free State. His research interests include physics, astrophysics, energy modeling, energy analytics, energy AI, and power systems.